Effect of Zn on microstructure evolution of Mg-Gd-Y-Nd-Zn-Zr alloy during heat treatment

Effect of Zn on microstructure evolution of Mg-Gd-Y-Nd-Zn-Zr alloy during heat treatment

T Li[1], D J Chen[2], W Liu[1] , J W Yuan[2], and J Qu[1]

1 China United Test &Certification Co., Ltd.,Guobiao(Beijing)Testing & Certification Co., Ltd., No.2, Xinjiekouwai Street, Xicheng district, Beijing, 100088, China
2 State Key Laboratory of Non-ferrous Metals and Processes, GRIMAT Engineering Institute Co., Ltd., No.11, Xinkedong Street, Huairou district, Beijing, 101407, China
E-mail: liting@gbtcgroup.com

Abstract. The effect of Zn on the microstructure evolution of Mg-7Gd-3Y-1Nd-xZn-0.5Zr (x=1.0, 2.0) (wt.%) alloys during homogenization and ageing heat treatment has been investigated systemically. The results indicate that as-cast 1 Zn alloy is composed mainly of α-Mg, Mg_5(RE, Zn) eutectic phase, $(Mg,Zn)_3$RE eutectic phase, stacking faults and block-like compounds rich in RE. Increasing of Zn content result in the disappearance of Mg_5(RE, Zn) eutectic phase, but the volume fraction of 14H-typ LPSO phase is increasing, which has made it even more difficult to dissolve into the matrix during homogenization. After homogenization at 520 ℃ for 48 h, the 14H LPSO phase remains in the alloys with 2 wt.% Zn, but only compounds rich in RE can be seen in the alloy with 1 wt.%Zn. After ageing at 240℃ for 18 h, the coherent β′ phase can be found both in 1Zn and 2Zn alloys, resulting in the increase of mechanical properties. The β′、β_1 and stacking faults can be found in 1Zn and 2Zn alloys after ageing at 240℃ for 100 h. However, it can be concluded that Zn can suppress the formation of LPSO phases but impede the precipitation of β′ and β_1 during the aging process. The as-aged alloy with 1% Zn addition shows the optimal mechanical properties.

1. Introduction

Magnesium alloys are attractive structural materials for automobiles, aircrafts, 3C products and biological fields, due to their low density, high specific strength and good damping capacity. Among these alloys, Mg–RE (rare earth) alloys with remarkable ageing responses is one of the most promising high strength Mg alloy. [1-4] Recently, Zn additions into Mg-RE alloys have widely been confirmed that will introduce LPSO structures, which can further improve the mechanical properties especially the ductility of magnesium alloys. The superior mechanical performance of Mg-RE-Zn alloy has been reported extensively. Kawamura et al.[5] firstly developed $Mg_{97}Zn_1Y_2$ alloys with high strength above 600 MPa and 5% elongation at room temperature through rapidly solidified powder metallurgy. Yamasaki et al. [6] reported a high strength hot-extruded Mg–2.3Zn–14Gd (wt.%) alloy with 345 MPa tensile proof strength and 6.3%. elongation. L. Zheng[7] produced Mg–10Gd–6Y–2Zn–0.6Zr alloy with the ultimate tensile strengths of 432 MPa and the elongations are 18% and 5% respectively.
Although there are many studies about the effect of Zn on the microstructure evolution and properties, there are still some disputes about the strengthening mechanism of Zn additions to Mg-RE alloys. T. Honma [8] considered that the Zn addition will enhance precipitations of the β′ phases and LPSO structures. The formations of these two phases minimize the total energy in the systems, leading to active movement of dislocations on the basal plane, which gives rise to the unusual elongation of Mg–2.0Gd–1.2Y–0.2Zr alloy. Yun Li[9] suggested that formation of LPSO phase increased the efficiency

of power dissipation and impeded the dynamic recrystallization, which causes Zn-containing alloys had stronger softening effects. Jinghuai Zhang[10] suggested that the kinking of LPSO structure is beneficial for both work hardening and plasticity, and 14H LPSO structure contributes more to the improvement of ductility while SF is more effective in increasing strength.

High strength Mg-7Gd-5Y-1Nd-0.5Zr alloys was fabricated in our previous work[11,12]. To further improve the ductility, Mg-Gd-Y-Nd-Zn-Zr alloy was developed by Zn addition recently[13-15]. In this alloy system, Zn was supposed to be mainly composed β_1 phases and LPSO structures but does not partition into β' phases[8], whereas Nd is reported that can impede the LPSO formation but enhance the solid solubility effect and peak-aging hardness[16]. Thus, the influence of Zn content on the microstructure and mechanical properties of Mg-Gd-Y-Nd-Zn-Zr alloys during heat treatment as well as the strengthening mechanism are essential to be studied.

The aim of this paper is to understand the influence of the Zn content in the Mg-Gd-Y-Nd-Zn-Zr system during heat treatment based on the microstructural observations and mechanical properties test. In addition, the precipitates in peak-aged alloys have been investigated for better understandings of the age-hardening mechanism.

2. Experimental procedures

Two alloys with nominal composition of Mg-7Gd-3Y-1Nd-1Zn-0.5Zr and Mg-7Gd-3Y-1Nd-2Zn-0.5Zr were prepared in high frequency induction melting furnace. The as-cast ingots were homogenized at 520 ℃ for 48h and aged at 210 ℃for 26 h. Microstructure observations were performed through scanning electron microscopy (SEM) equipped with EDS and transmission electron microscopy (TEM). Disc samples (3 mm diameter) for TEM analyses were ground to 60 μm thick and then twin-jet electro-polished in a solution of 15 mL perchloric acid and 285 mL ethanol at -30 ℃ and 0.01 A. The microstructures were observed by JEM-2010 HRTEM, HAADF-STEM images were taken using a FEI Tecnai F20 electron microscope. The mechanical properties of these two alloys were tested using the SANS machine at a speed of 2 mm/min at ambient temperature.

3. Results and discussion

3.1. As-cast microstructures

Fig. 1 shows the XRD patterns of the as-cast alloys. The as-cast 1Zn alloy is mainly composed of α-Mg, Mg_5(RE, Zn) (Mg, Zn)$_3$RE phase, and Mg_{12}(RE, Zn) phases, as seen from Fig. 1. Otherwise, in as-cast 2Zn alloy, disappearance of Mg_5(RE, Zn) phase can be recognized from the results. The intensity of the diffraction peaks for Mg_{12}(RE, Zn) is much stronger in as-cast alloys.

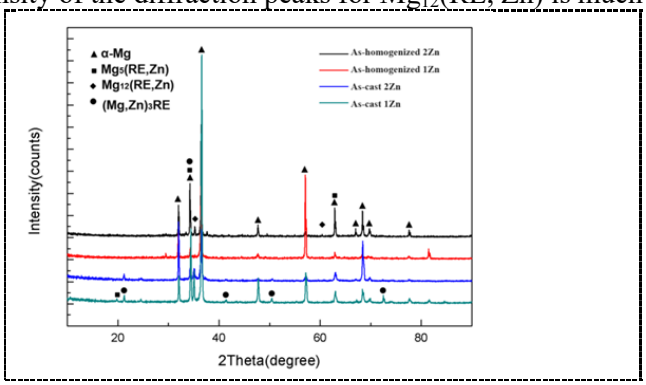

Figure 1. XRD patterns of as cast 1Zn and 2Zn alloy

Fig.2 shows as-cast microstructure of 1Zn and 2Zn alloys. As seen in Fig.2a, the eutectic phase (indicated by A and B), and square shaped compounds (indicated by C) rich in Gd and Y distribute along the grain boundaries in 1Zn alloy. Besides, a number of needle-like structures near grain boundaries which distribute along the same direction can also be found. According to XRD and EDS results, the eutectic phase A and B can be designated as Mg_5(RE, Zn) and (Mg, Zn)$_3$ RE, respectively. In 2Zn alloy, it is found that the characteristics of the eutectics such as (Mg, Zn)$_3$ RE and compounds rich in Gd/Y are same to that of the phases observed in the as-cast 1 Zn alloy, which is consistent with the XRD patterns. The difference is only that the disappearance of Mg_5(RE, Zn) phases. The addition

of 2% Zn has made more needle-like structure precipitated throughout all the grains. Moreover, besides these similar phases, $(Mg, Zn)_{12}RE$ phase can be observed in 2Zn alloy, which is not found in the microstructure of 1Zn alloy as shown in Fig.2a, although the diffraction peaks for $Mg_{12}(RE, Zn)$ in 1Zn alloy can be found as shown in Fig.1.

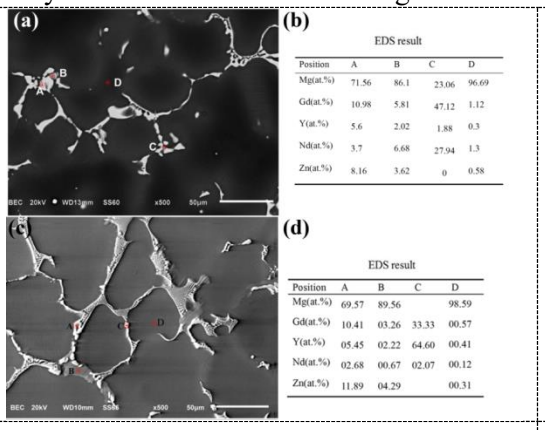

Figure 2. (a) SEM image of as-cast 1Zn alloy; (b) EDS results of the compounds marked by A, B C, D in Fig.2a; (c) SEM image of as-cast 2Zn alloy; (b) EDS results of the compounds marked by A, B C, D in Fig.2c

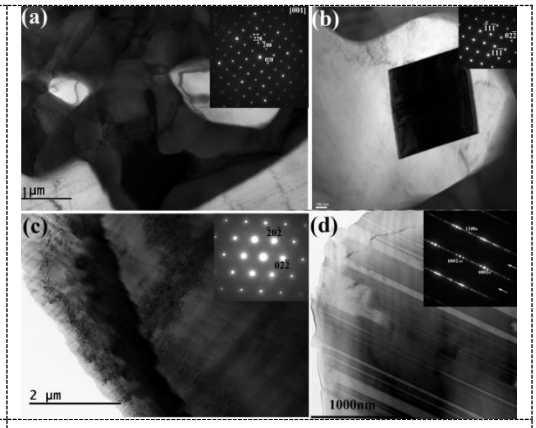

Figure 3. (a) bright field TEM image and corresponding SAED pattern of eutectic phase B in 1Zn alloy; (b) bright field image and corresponding SAED pattern of secondary phase C; c) bright field image and SAED pattern of A in 2Zn alloy; d) bright field image and SAED pattern of LPSO in 2Zn alloy

TEM and SAED analysis for eutectic phase B and compounds C was conducted, as shown in Fig.3. The SAED pattern shown in Fig.3a indicates the skeletal eutectic phase B formed along grain boundaries can be deduced as f.c.c. crystal structure with a=2.22 nm. The square-shaped compounds C shown in Fig. 1(a) is determined to be f.c.c. crystal structure with a lattice parameter of a=0.53 nm. It is obvious that the eutectic phase B and compounds C is similar to that formed in Mg-RE series alloy in our previous research [13]. Moreover, $(Mg, Zn)_3RE$ phase observed in 1Zn alloy that is distinguish with 2Zn alloy was analyzed by TEM and HRTEM, as shown in Fig.3c. The $(Mg, Zn)_3RE$ phase in 1Zn and 2Zn alloy have been determined to present a f.c.c. with a=0.73 nm. Furthermore, TEM image and SAED pattern of LPSO structure in 2Zn alloy are shown in Fig. 3d, The SAED pattern viewed along $[11\bar{2}0]_\alpha$ axis of LPSO phase indicate that the present LPSO phase formed during solidification is 14H-type with a lattice parameter of a=1.112nm，c=3.647nm. The orientation relationship between 14H-type LPSO structure and matrix can be described as $(0001)_{14H}//(0001)_\alpha$, $[01\bar{1}0]_{14H}//[\bar{1}\bar{1}20]_\alpha$. This 14H-type structure considered to be the same as the 14H-type structure reported by Zhu[18].

3.2. As-homogenized microstructures

Fig. 4 shows the differential scanning calorimetry (DSC) curves of the as-cast alloys. As seen from Fig.4, the melting points of eutectics are evaluated to be approximately 537.1℃, 529.3 ℃ for 1Zn and 2Zn alloy, respectively. With increase of Zn content, the melting point of eutectics is decreased and the endothermic peak area increase significantly Zn, which is consistent with XRD results shown in Fig.1. According to the DSC results, the subsequent homogenization heat treatment for both 1Zn and 2Zn alloys is performed at 520 ℃ for 32 h.

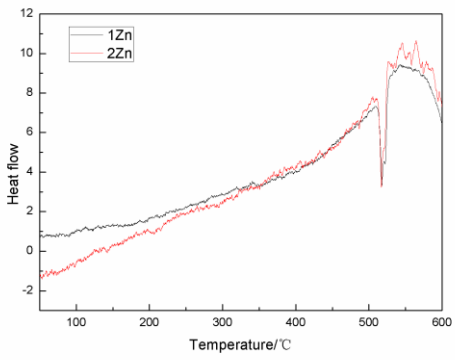

Figure 4. The differential scanning calorimetry curves of 1Zn and 2Zn alloy

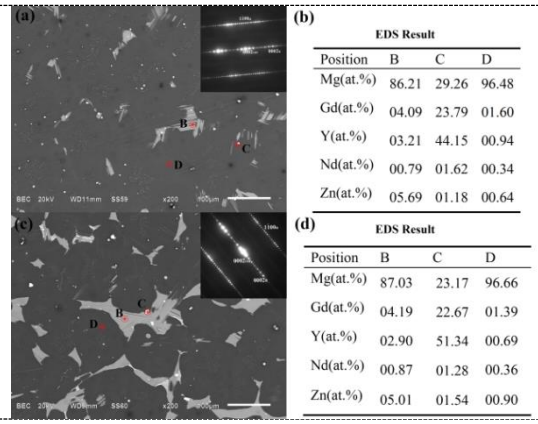

Figure 5. (a) SEM image of as-homogenized 1Zn alloy; (b) EDS results of the compounds marked by B C, D in Fig.1a; (c) SEM image of as-homogenized 2Zn alloy: (b) EDS results of the compounds marked by B C, D in Fig.1c

Fig.5 shows the microstructure of as-homogenized alloys. After homogenization heat treatment at 520 ℃ for 32 h, the eutectic phase has been completely dissolved into matrix. However, the LPSO along grain boundaries both in 1Zn and 2Zn alloy can be seen in Fig.5a and Fig.5c. With increasing of Zn content, the volume fraction of LPSO phase is increasing, which has made it even more difficult to dissolve into the matrix during homogenization. As shown in the illustrations in Fig.5a and Fig.5c, 14H LPSO structure can be deduced from the SAED pattern. Thus, the undissolved block shaped phase is LPSO with 14H-type structure. The as-homogenized microstructures of 1Zn and 2Zn alloys are mainly composed of α-Mg, secondary phase rich in RE and 14H-type LPSO phase. The research by Zhu et al. [18] revealed that the stable structure of $Mg_{12}YZn$ in the solid solution Mg–Y–Zn alloy was 14H-LPSO. For 1Zn alloy, needle-like structures near grain boundaries transformed into block LPSO phase, and LPSO phase in 2Zn alloy is much larger after homogenization. The similar phenomenon was reported by Yamasaki et al.[19], and there are many other standpoints about the formation mechanism of 14H-LPSO during homogenization heat treatment, such as precipitation from α-Mg matrix, or transformed from different type of LPSO, or decomposition of eutectic phases. However, in the present study, it is hard to distinguish the mechanism of 14-H LPSO phase coarsening, and further research has to be studied to understand the coarsening mechanisms of the 14H-LPSO during homogenization.

3.3. As-aged microstructures

To reveal the microstructure of as-aged alloys, TEM was conducted for 1Zn alloy and 2Zn alloy. Fig. 6(a) shows a low-magnification TEM image of 1Zn alloy after 240 ℃/18 h ageing, taken with the incident beam parallel to $[0001]_\alpha$. The microstructure is mainly composed of fine precipitates formed on $(11\bar{2}0)_\alpha$ planes. The corresponding SAED pattern taken from both the matrix and precipitates shown in Fig. 6(b) can be indexed consistently with b.c.o. structure with a=0.64 nm, b=2.22 nm and c=0.52 nm. The bright field image and SEAD pattern both suggested that β′ phases have formed during aging process in 1Zn alloy. Besides β′ phase which has the same structure with that in EW75 alloy in our previous work, some clusters marked by arrows has found in matrix. These clusters has a hexagonal shape, Nie has reported and thought they are short-range order [20]. In future work, the crystal structure of this cluster will be further investigated.

The TEM image viewed along the $[11\bar{2}0]_\alpha$ zone axis for the 1Zn alloy after 240 ℃/100h ageing are shown in Figs. 6(d). Viewing from the $[11\bar{2}0]_\alpha$ direction, all the β′ precipitates are parallel to $[0001]_\alpha$ direction. In addition, compared with 1Zn alloy, the microstructure of 2Zn alloy shown in Fig. 6c and Fig.6f indicate that with increasing of Zn content, the fewer β′ phases has formed in matrix. This result

can be ascribed to the larger amount of residual LPSO phase in 2Zn alloy. As a second phase, the composition of 14H-type LPSO is approximate $Mg_{12}Zn_1RE_1$. The residual LPSO phase in homogenized alloy consumed Gd, Y and Nd atoms, which result in the fewer β′ phases precipitated from matrix during ageing.

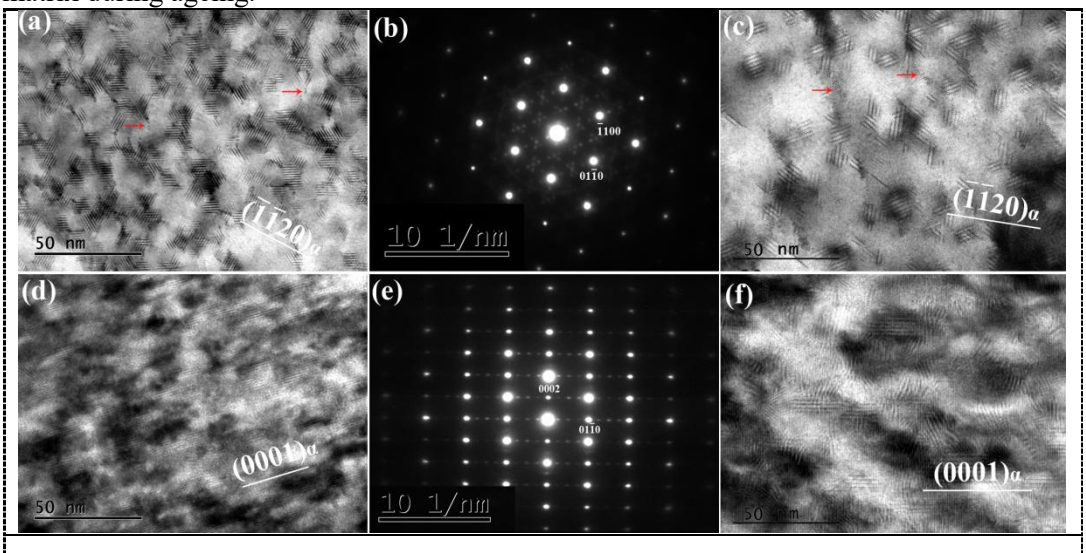

Figure 6. TEM images of samples aged at 240 ℃ for 18h (a) bright field image of 1 Zn alloy taken along$[0001]_\alpha$; (b) SAED pattern corresponding to a; (c) bright field image of 2 Zn alloy taken along $[0001]_\alpha$; (d) bright field image of 1 Zn alloy taken along$[11\bar{2}0]_\alpha$; (e) SAED pattern corresponding to d; (f) bright field image of 2 Zn alloy taken along $[11\bar{2}0]_\alpha$

To investigate precipitates formed after continued ageing at 240 ℃ for 100 h in 1Zn alloy, HAADF-STEM technique was adopted. The HAADF-STEM images for 1Zn alloy after 240 ℃/100 h ageing are shown in Fig. 7(a) and 7(d), respectively. Viewing from $[0001]_\alpha$ zone axis, a large amount of coarse β′ precipitates can be observed in Fig. 7(a). The size of β′ precipitate along $[0001]_\alpha$ direction is about 100nm. The FFT pattern inserted in Fig. 7(c) shows that the structure of β′ precipitates not change during ageing. Besides β′ phase, another phase with a pair of facets parallel to $\{1\bar{1}00\}_\alpha$ planes and the other pair of facets attached to β′ can be found, which was marked in Fig.7(a). Closer examination revealed that the habit of this precipitation is $(1\bar{1}00)_\alpha$. FFT recorded from such precipitates, as shown in Fig. 7(c), could be indexed consist with β_1 phase(f.c.c, a=0.74nm) . An HAADF-STEM image for 1Zn alloy taken with the incident beam parallel to $[11\bar{2}0]_\alpha$ is shown in Fig. 7(d). Besides β′ and β_1 phase, some needle-like structures perpendicular to $[0001]_\alpha$ direction can be observed. FFT pattern of this structure is shown in Fig.7f, strong streaks indicate the existence of stacking fault. HAADF-STEM observation (Fig. 7d) reveals that solute elements such as Zn and Gd concentrate in stacking faults. The high resolution TEM image of SF (Fig. 7f) shows a stacking sequence of ABABACBCBC of the closely packed plane. The interaction of β′ and SF can also be found, and our further work will be done to investigate the interface between β′, β_1 and SF structures.

Based on the Z-contrast mechanism in HAADF technique, we can associate the fact that the RE and Zn concentrate in β′, β_1 phase and SF structure, and the content of RE in β_1 phase is higher than that in β′ phase. Precipitations in 2Zn alloy after ageing at 240 ℃ for 100 h are shown in Fig. 7(b) and 7(e), respectively. A HAADF-STEM image taken with the incident beam parallel to $[11\bar{2}0]_\alpha$ in Fig. 7(b) and 7(e) show that with increasing of Zn content, the fewer β′ and β_1 phases formed in matrix, but

higher density of SF can also can be found. This result can be ascribed to the larger content of Zn in 2Zn alloy, thus the SF formed easily. Due to the SF contains Gd, Y and Nd atoms, which result in the fewer RE in matrix in 2Zn alloy and fewer β′ and β_1 phases formed in matrix.

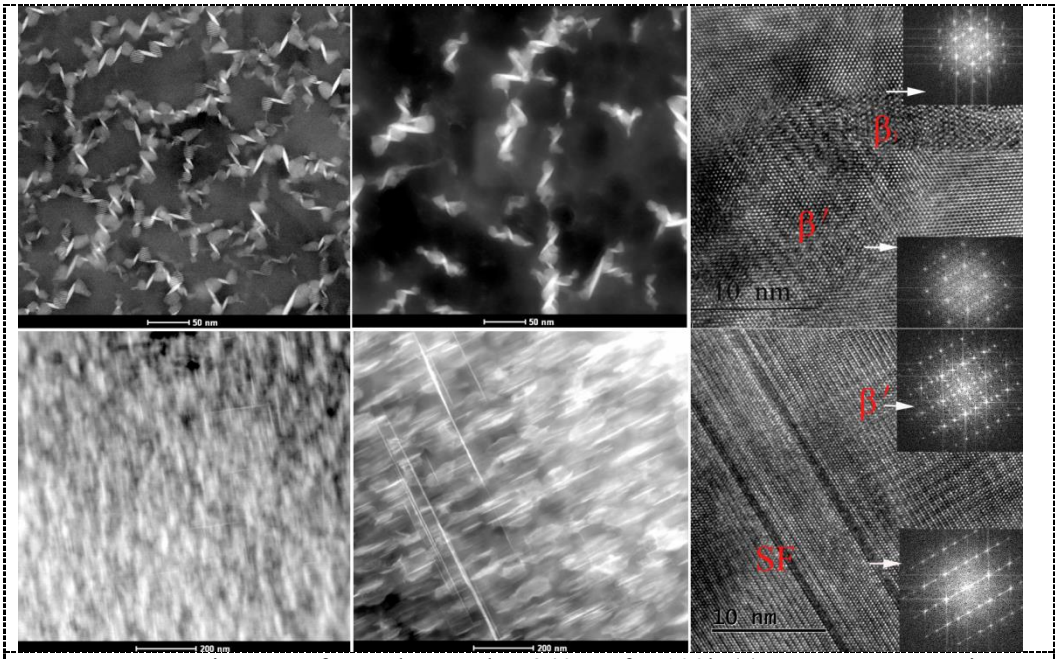

Figure 7. TEM images of samples aged at 240 ℃ for 100h (a) HAADF-STEM image of 1 Zn alloy taken along $[0001]_\alpha$; (b) HAADF-STEM image of 2 Zn alloy taken along $[0001]_\alpha$; (c) HRTEM image of 1 Zn alloy taken along $[0001]_\alpha$; (d) HAADF-STEM image of 1 Zn alloy taken along $[11\bar{2}0]_\alpha$; (e) HAADF-STEM image of 2 Zn alloy taken along $[11\bar{2}0]_\alpha$; (f) HRTEM image of 2 Zn alloy taken along $[11\bar{2}0]_\alpha$

3.4. Mechanical properties

The mechanical properties such as yield strength (YS), ultimate tensile strength (UTS) and elongation for 1Zn and 2Zn alloy before and after heat treatment has been tested. The as-cast 2Zn alloy exhibits lower mechanical properties and the UTS, YS and elongation are 172MPa 128MPa, and 2.8, respectively. After homogenization and 100 h ageing heat treatment, the UTS, YS and elongation for 1Zn alloy are 298 MPa, 233 MPa and 10.3, respectively. The UTS, YS and elongation for 2Zn alloy are 274 MPa, 198 MPa and 12.5, respectively. The lower strength for as-aged Mg-7Gd-5Y-1Nd-2Zn-0.5Zr alloy is attributed to the fewer β′ and β_1 phases formed during ageing. However, the higher density of SF result in the higher elongation for as-aged 2Zn alloy.

4. Conclusions

In this study, the effect of Zn on the microstructure evolution of Mg-7Gd-3Y-1Nd-xZn-0.5Zr (x=1.0, 2.0) (wt.%) alloys during homogenization and ageing heat treatment has been investigated systemically, the main conclusions can be summarized as follows:

1) As-cast 1 Zn alloy is composed mainly of α-Mg, Mg_5(RE, Zn) eutectic phase, $(Mg,Zn)_3RE$ eutectic phase, stacking faults and block-like compounds rich in RE. Increasing of Zn content result in the disappearance of Mg_5(RE, Zn) eutectic phase, but 14H-type LPSO phase can be found in as-cast 2Zn alloy.

2) After homogenization heat treatment of 520 ℃ for 32 h, the eutectic phase has been completely dissolved into matrix. However, the 14-H type LPSO phases distributed along grain boundaries both in 1Zn and 2Zn alloy. The variation of morphology and size of LPSO during homogenization can be found.

3) After 240 ℃/18 h ageing, β′ phase has precipitated from matrix. Some hexagonal shaped clusters with a hexagonal structure have also been found in 1Zn alloy. After continued ageing at 210 ℃ for 100 h, a large volume fraction of coarse β′ precipitates can be observed. Besides, β_1 phase with higher RE content can also be found.

4) With increasing of Zn content, the fewer β′ and β_1 phases formed in 2Zn alloy, but higher density of SF can also be found. As a result, the strength of as-aged 2Zn alloy is lower but elongation is higher.

5. References

[1] Aderhold J, Davydov V Yu, Fedler F, Klausing H, Mistele D, Rotter T, Semchinova O, Stemmer J and Graul J 2001 *J. Cryst. Growth* **222** 701
[1] Lorimer G W, Apps P J, Karimzadeh H, and King J F, Mater. Sci. Forum 419–422 279
[2] Smola B, Stulikova I, Vonbuch F, Mordlike B L, Mater. Sci. Eng. A 324 113
[3] Peng Q M, Hou X L, Wang L D, Wu Y M, Cao Z Y, Wang L M, Mater. Des. 30 292
[4] Smola B, Joska L, Brezina V., Stul ́kov á I., Hnilica F., Mater. Sci. Eng. C 32 659
[5] Kawamura Y, Hayashi K, Inoue A, Mater. Trans. 42 1171
[6] M. Yamasaki, T. Anan, S. Yoshimoto, Y. Kawamura, Scripta Mater. 53 799
[7] Zheng L, Liu C M, Wan Y C, Yang P W, Shu X. J. Alloys Compd. 509 8832
[8] Honma T, Ohkubo T, Kamado S, Hono K. Acta Mater., 55 4137
[9] Li Y, Xiao W L, Wang F, Hu T, Ma C L. J. Alloys Compd., 745 33
[10] Zhang J H, Leng Z, Liu S J, Li J Q, Zhang M L, Wu R Z. J. Alloys Compd. 509 7717
[11] Xia X S, Chen Q, Zhao Z D, Ma M L, Li X G, Zhang K. J. Alloys Compd., 623 62
[12] Li T, Du Z W, Zhang K, Li X G, Yuan J W, Li Y J, Ma M L, Shi G L, Fu X, Han X L, J. Alloys Compd., 574 174
[13] Li M, Zhang K, Du Z W, Li X G, Li Y J, Ma M L, Shi G L, Yuan J W, Li T, Liu J B. Mater. Charact. 109 (2015) 66–72.
[14] Li M, Zhang K, Du Z W, Li X G, Li Y J, Ma M L,. Trans. Nonferrous Met. Soc. China 26(2016) 1835−1842.
[15] Li M, Zhang K, Li X G, Li Y J, Ma M L, Shi G L, Yuan J W, Li T, Liu J B. Mater. Sci. Eng.A 626 415
[16] Zhang X G, Meng L G, Fang C F, Peng P, Ja F, Hao H, Mater. Sci. Eng. A 586 19
[17] Metallic materials-tensile testing-part 1: method of test at room temperature (ISO6892-1: 2009, MOD), GB/T 228.1-2010, p. 35.
[18] Zhu Y M, Morton A J, Nie J F: Acta Mater. 60 6562
[19] Yamasaki M, Sasaki M, Nishijima M, Hiraga K, and Kawamura Y: Acta Mater. 55 6798
[20] Nie J F, Wilson N C, Zhu Y M, Xu Z. Acta Mater. 106 260-271

Acknowledgments

This work was supported by the Natural Science Foundation of China (No. 51501015, No. 51871195), Jinqiao Seed Foundation of Beijing, and National Basic Research Program of China (No. 2013CB632202)